4*p*-inner-shell and double-excitation spectrum of Sr II

C. Banahan, J. T. Costello, D. Kilbane, and P. van Kampen
National Centre for Plasma Science and Technology and the School of Physical Sciences, Dublin City University, Glasnevin, Dublin 9, Ireland

(Received 11 November 2008; published 12 February 2009)

We report photoabsorption measurements from the 4*p* inner shell of singly ionized strontium in the spectral region between 26.0 and 37.4 eV. More than 60 levels of Sr II are reported which are interpreted as singly excited inner-shell transitions $4p^6 5s\ ^2S_{1/2} \rightarrow 4p^4 5s(^1P, ^3P)ns$, *md* and doubly excited transitions $4p^6 5s\ ^2S_{1/2} \rightarrow 4p^5 4d(^1P, ^3P, ^3D)nl$. Multiconfiguration Hartree-Fock calculations are performed in *jj* coupling and the levels are arranged into Rydberg series converging on seven limits, allowing the identification of two levels in Sr III.

DOI: 10.1103/PhysRevA.79.022509 PACS number(s): 31.10.+z, 32.30.Jc, 32.70.Cs, 32.80.Fb

I. INTRODUCTION

Inner-shell photoionization in atoms and ions has maintained interest throughout the years as it provides insight into the correlation effects that occur near threshold: interchannel coupling, relaxation, exchange, Auger decay, etc. In this context, excitation and ionization of the highest filled *p* subshell in alkaline-earth metals are of particular interest, as previous studies show [1–7]. Due to electron-electron correlation between the inner and valence shells, one observes excitation of one or both valence electrons simultaneously. As a consequence, a wealth of structure is observed making identification of lines difficult and testing for theoretical codes .

Previous theoretical studies using multiconfiguration Hartree-Fock (MCHF) and Hartree-Fock with exchange (HFX) calculations in *LS* coupling have provided accurate results for *p*-subshell excitation in both Ca I [6] and Sr I [2]. The overall distribution of intensity was well explained by the consideration of $np^6(n+1)s^2 \rightarrow np^5(n+1)s^2 md$, *ms* ($n=3$ for Ca, 4 for Sr, and $m \geqslant n$) transitions. To account for the large number of lines observed, multielectron excitation needed to be considered. Double excitations of the type $np^5 nd^2(n+1)s/d$ were found to be the most significant. Separate minimization calculations were necessary for the $np^5 nd(n+1)s^2\ ^1P$ terms to account for the potential barrier that repels the *d* wave function out of the core, an effect first noted by Hansen [8] in his study of the Ar I isoelectronic sequence.

The 5*p* excited spectrum of Ba I caused controversy due to discrepancies between the observed spectrum and theoretical predictions. Anomalies concerning the double to single photionization rates were reported [9,10]; subsequent proposed explanations differed [11–13]. A detailed study of the 5*p* photoabsorption structure by Connerade *et al.* [14] and Rose *et al.* [15] unraveled the mystery of the double-ionization process. The former group classified series converging to 12 limits of Ba II which agreed well with binding energy measurements for the 5*p* shell of Ba I obtained by Mehlhorn *et al.* [16] by electron impact spectroscopy. Rose *et al.* [15] successfully applied a fully relativistic *ab initio* multiconfiguration Dirac-Fock (MCDF) procedure to assign six series limits observed in [14,16]. They found that final ionic state configuration interaction (FISCI) calculations provided accurate energy values and intensities for the most prominent peaks in the electron-impact 5*p* ionization spectrum. On the basis of their analysis, the energy viability of two-step autoionization was established, as had been predicted [12,17].

However, in the case of the singly ionized counterparts, accurate theoretical results have proven more difficult to obtain. Hansen [12] showed that it was necessary to include exchange in his calculations to properly account for the observed electron-impact ionization functions of Mg II, Ca II, Sr II, and Ba II. The measured electron-impact ionization functions for Mg II, Ca II, Sr II, and Ba II displayed remarkable differences for the $p^5 ds$ excitations [18]. The ionization cross sections for Ca II, Sr II, and Ba II exhibited abrupt thresholds, indicating strong contributions from autoionization, while there was no evidence for this in Mg II. Moores and Nussbaumer [19] proposed that this was due to the fact that the largest autoionization contribution arose from the $2p \rightarrow 3p$ transition, where $\Delta n=1$. Since the two electrons have different principal quantum numbers, the overlap between their wave functions is much smaller than in the other alkaline earths where $\Delta n=0$ for the $p^5 ds$ transitions.

Theoretical analysis of the Ca II spectrum was first carried out by Miezcnik *et al.* [20] using the *R*-matrix method. They managed to successfully reproduce the 3*p*-3*d* shape but not the other structure present. Ivanov and West [21] used the spin-polarized version of the random phase approximation with exchange (RPAE) method to corroborate previous identifications of the main one-electron transitions [20,22]. However, they were unable to account for two-electron excitations which appeared prominently in the spectrum. Hibbert and Hansen [23] carried out a large-scale *ab initio* CI calculation using the *R*-matrix method and succeeded in identifying most of the structure observed in Ca II ions.

Although the first 5*p* photoabsorption spectrum of Ba II was recorded over 30 years ago by Roig *et al.* [24], much of the structure remains unidentified. Absolute photoionization cross section measurements were made by Lyon *et al.* [25] in 1987 and some identifications were possible by comparing the limits of series observed in [14] for the neutral atom. A similar predicament is noted for singly ionized strontium.

As discussed above, several studies of Sr I have led to significantly improved agreement between theory and ex-

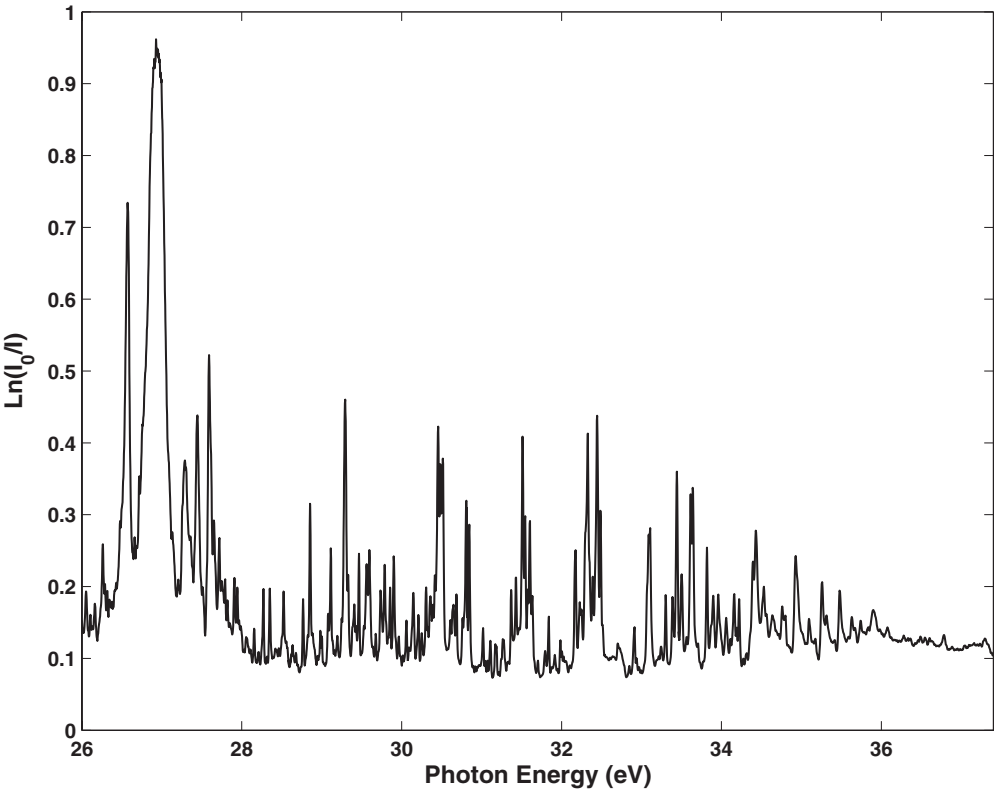

FIG. 1. The $4p$ inner shell photoabsorption spectrum of Sr II recorded 1 mm from the target surface and 500 ns after plasma generation.

periment [2,26,27], but only a small number of studies have been made on Sr II: electron impact ionization [18,28,29] studies, $3d$ photoabsorption spectra of Sr I–IV by McGuinness *et al.* [30] and photoion-yield spectra from the $3d$ excited states of Sr II by Itoh *et al.* [31]. Employing a multiconfiguration Dirac-Fock calculation, Itoh *et al.* deduced that the numerous discrete lines observed in the spectra were due to strong $5s$-$4d$ mixing: After the $3d$ hole creation, the $4d$ wave function collapses and strong mixing occurs due to the now close proximity of the $4d$ and $5s$ orbitals. Mansfield and Newsom [2] photographed the Sr I spectrum and proposed 18 series limits which were also observed by White *et al.* [29] as ejected-electron lines, thus providing tentative assignments of 18 Sr II levels. Lyon *et al.* [32] employed the merged beam technique to measure absolute photoionization cross sections of Sr II. Using the previous studies mentioned above, they also compared their measurements with the results of Hansen [12] who employed Hartree-Fock (HF) and MCHF calculations. Hansen positioned the main resonance $(4p^5 4d\ ^1P)5s\ ^2P$ at 27.13 eV (HF) and 26.77 eV (MCHF) and Lyon measured a doublet positioned at 26.950 and 26.972 eV, in good agreement with Hansen's prediction. The cross section was dominated by a large number of autoionizing resonances which they did not assign to any configuration.

In this study, the $4p$ photoabsorption spectrum of Sr II has been measured in the photon energy range 26.0–37.4 eV. Over 60 lines have been identified and ordered into Rydberg series converging onto seven limits with the aid of a MCHF calculation in the jj coupling scheme.

II. EXPERIMENT

The strontium spectra were recorded electronically using the dual laser plasma (DLP) technique, which involves the generation of both the absorbing species of interest and a synchronized bright backlighting source using two laser produced plasmas [33]. The strontium plasma was created by focusing a 410 mJ, 15 ns Nd:YAG laser pulse onto a strontium target to a line of length 4 mm, while a second Nd:YAG laser pulse (~0.58 J in 15 ns) was tightly focused (~60 μm spot diameter) onto a tungsten target to serve as the backlighting continuum emitting plasma. Radiation from this plasma is collected by a toroidal mirror and imaged onto the 20 μm entrance slit of a 2.2 m McPherson grazing incidence vacuum spectrograph. The detector consists of a 40 mm microchannel plate coupled via a coherent optic fiber bundle to a 1024 pixel photodiode array with an energy resolution $\frac{E}{\Delta E}$ better than 700. The temporal resolution of the system is 4 ns. The spectra were calibrated against known emission lines of aluminum, manganese and oxygen ions.

Variation of the time delay Δt between the generation of the two plasmas allowed us to monitor the temporal evolution of the plasma. By selecting a distance Δx from the target surface in conjunction with a chosen time delay, we could successfully isolate a region in the plasma predominantly comprised of the strontium ion. In this experiment the optimum parameters to isolate Sr II were $\Delta t = 500$ ns and $\Delta x = 1$ mm.

III. DISCUSSION OF RESULTS

The Sr II $4p$ subshell spectrum is presented in Fig. 1. Using the Cowan suite of codes [34,35], we performed multiconfiguration interaction calculations for the following transitions:

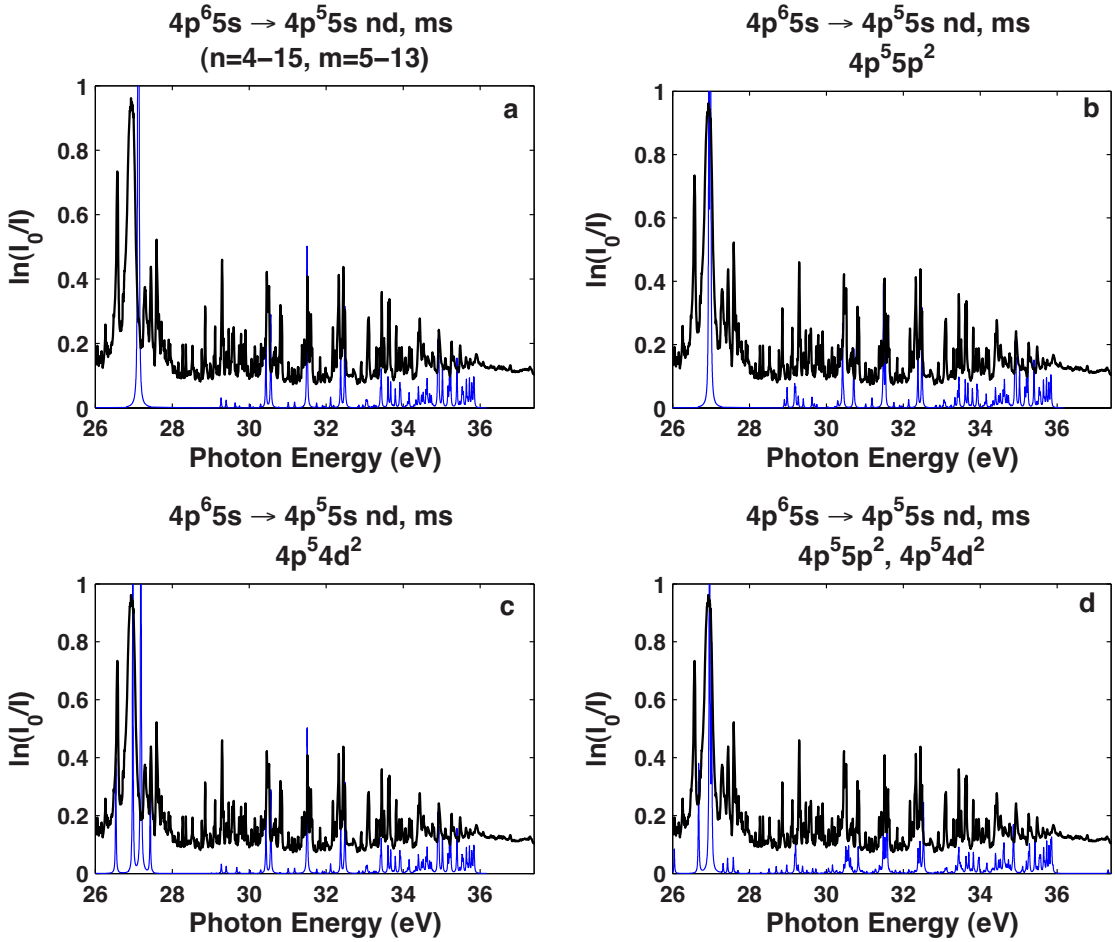

FIG. 2. (Color online) Photoabsorption spectrum of Sr II (black) with the separately calculated spectra to show the effect of the $5p^2$ and $4d^2$ configurations on the p^5ds level. (a) Transitions to the $4p^55s\,nd$, ms level without configuration interaction. The predicted energy for the main resonance is slightly higher than observed. (b) The same as (a) including the $4p^55p^2$ configuration. The main resonance has shifted down to lower energy, matching the experimental value well. Notice a redistribution of oscillator strength also, a reduction can be seen around 30–32 eV and some new peaks are observed ~29 eV which can be attributed to the $5p^2$ configuration. (c) The same as (a) including the $4p^54d^2$ configuration, the appearance of peaks to the left and right of the main resonance confirm their identification as belonging to this configuration. (d) The full calculation performed which gives good overall agreement with the observed photoabsorption spectrum (metastable contribution is not included and but account for the other peaks). All lines in the theoretical plot have been fitted with a Lorentzian width of 0.02 eV to match experiment.

$$
\begin{aligned}
4p^6 5s &\rightarrow 4p^5 5snd \quad (4 \leqslant n \leqslant 15)\\
&\rightarrow 4p^5 5sms \quad (5 \leqslant m \leqslant 13)\\
&\rightarrow 4p^5 4dns \quad (5 \leqslant n \leqslant 10)\\
&\rightarrow 4p^5 4dmd \quad (4 \leqslant m \leqslant 10)\\
&\rightarrow 4p^5 5p^2,
\end{aligned}
$$

$$
\begin{aligned}
4p^6 4d &\rightarrow 4p^5(5s+4d)ns \quad (5 \leqslant n \leqslant 10)\\
&\rightarrow 4p^5(5s+4d)md \quad (4 \leqslant m \leqslant 10)\\
&\rightarrow 4p^5 5p^2.
\end{aligned}
$$

The Slater-Condon parameters were reduced to optimize the theoretically calculated transitions with experiment as follows: R integrals by 15%, F integrals between equivalent electrons by 15%, and by 10% for nonequivalent electrons. The G integrals were reduced by 22% and the ζ integrals were left unchanged. Reductions in the range 5–25 % are required to allow for configuration-interaction effects not included explicitly in the calculation [35]. The above reductions in this case provided the best estimate of the energy separations observed in the spectrum. A separate minimization calculation for the $(4p^54d\ ^1P)5s$ configuration was not needed for Sr II although it was necessary for Ca I, II [6,20] and Sr I [2]. We suggest that this is probably due to the greater extent of $4d$ wave function collapse. As a result, strong configuration mixing between the $4p^55snd$, ms and $4p^54dnd$, ms levels is expected. Figure 2(a) displays the results of the $4p$ excited calculations of the $4p^65s \rightarrow 4p^55snl$ transitions only. A different intensity distribution is apparent and fewer transitions are noted, providing further validation for the inclusion of configuration interaction with the $4p^54dnd$, ms levels.

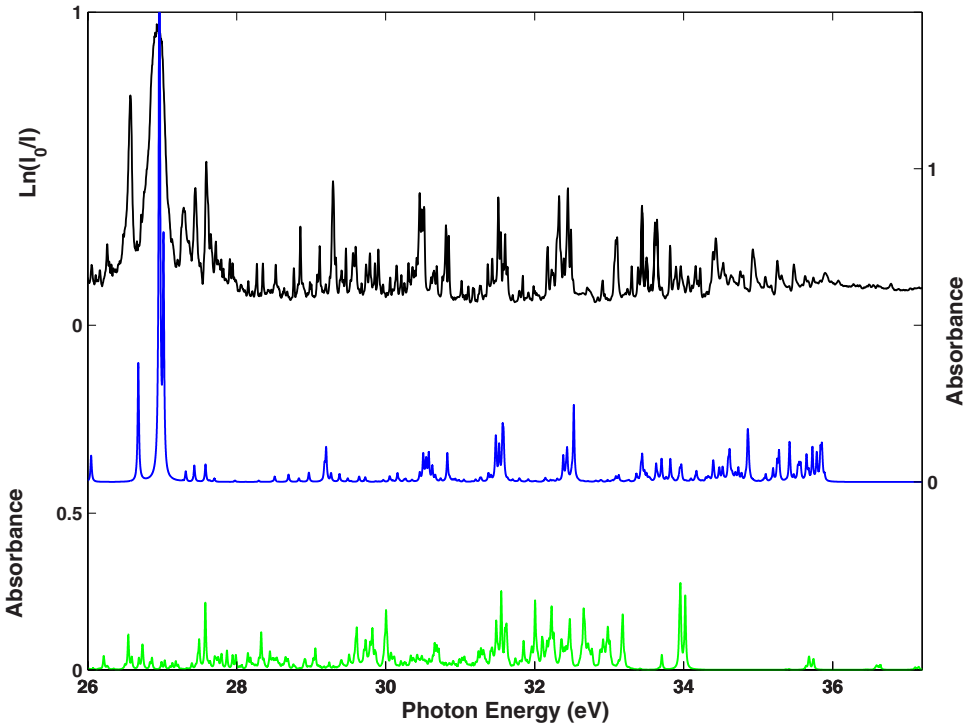

FIG. 3. (Color online) Photoabsorption spectrum of Sr II (top) with the separately calculated ground state absorption (middle) and metastable spectrum from the $4p^6 4d\ ^2D_{3/2,5/2}$ states (bottom). All lines in the theoretical plot have been fitted with a Lorentzian width of 0.02 eV to match the experimental spectrum.

The *jj*-coupling scheme was favored over the $[J_c]$K and *LS* coupling schemes as it gave the best overall fit to the experimental results. Although *LS*, *jj* and $[J_c]K$ percentage purities were comparable (36.0%, 46.0%, and 30.3%, respectively), neither scheme properly predicted ordered Rydberg series thus the labeling assigned in the tables is based on the quantum defect values and estimated Rydberg series limits.

Hansen [12] found that the $p^5ds \leftrightarrow p^5p'^2$ interaction plays an important role in p^5ds configurations in Sr II through configuration interaction. The $p^5ds \leftrightarrow p^5p'^2$ interaction is largest in the $(^1P)^2P$ state. Hansen explained that due to the expansion of the *d* orbital in the $(^1P)^2P$ state, considerable overlap between the *d*, *s*, and *p'* orbitals occurs; in effect the radial interaction integral is a factor of 2 larger for $(^1P)^2P$ than for $(^3P)^2P$. The $p^5ds \leftrightarrow p^5s^2$ interaction was also found to be important for the $(4p^5 4d\ ^3P)5s\ ^2P$ state due to the near coincidence between the two states. Figure 2 displays the results of multi-configuration Hartree-Fock calculations with and without the $5p^2$ and $4d^2$ configurations. One can see the effect of including the $4p^5 5p^2$ configuration, with a better energy observed for the large resonance $[(4p^5 4d\ ^1P)5s\ ^2P$ levels] positioned ~27 eV. The inclusion of the $4p^5 4d^2$ configuration correctly predicts the strong lines observed on either side of the dominant resonance.

The first excited states of Sr II, $4p^6 4d\ ^2D_{3/2,5/2}$, lie a mere 1.805 and 1.840 eV respectively, above the ground state.

TABLE I. A comparison between energy values and the corresponding label for the $4p^5 4d\ 5s$ configuration in both *LS* and *jj* coupling. The first column displays the *jj* coupling transition assignments but in *LS* designation for ease of comparison with the *LS* coupling results. In *LS* coupling, one can see better designation agreement with previous results [2,32].

jj coupling *LS* designation	Energy (eV)	*LS* coupling *LS* designation	Energy (eV)	Lyon (eV)	Mansfield (eV)
$(^3P)^4P_{1/2}$	21.137	$(^3P)^4P_{1/2}$	21.137		21.224
$(^3P)^4P_{3/2}$	21.275	$(^3P)^4P_{3/2}$	21.275	21.37	21.363
$(^1P)^2P_{1/2}$	21.702	$(^3P)^2P_{1/2}$	21.702	21.81	21.804
$(^3D)^4D_{3/2}$	21.820	$(^3P)^2P_{3/2}$	21.820	21.915	21.914
$(^1D)^2D_{3/2}$	22.466	$(^3F)^4F_{3/2}$	22.466		
$(^3P)^2P_{1/2}$	23.690	$(^3D)^4D_{1/2}$	23.691		
$(^3P)^2P_{3/2}$	23.694	$(^3D)^4D_{3/2}$	23.694		
$(^3P)^2P_{1/2}$	23.836	$(^1D)^2D_{3/2}$	23.836		
$(^3D)^2D_{3/2}$	24.860	$(^3D)^2D_{3/2}$	24.860		
$(^1P)^2P_{3/2}$	26.962	$(^1P)^2P_{3/2}$	26.962	26.972	
$(^3D)^4D_{1/2}$	27.017	$(^1P)^2P_{1/2}$	27.017	26.95	

TABLE II. Experimental and calculated series limits for the 4*p* subshell of Sr II.

Series Limit	No.	Banahan (eV)	Persson (eV)	Reader (eV)	Kilbane (eV)	Hansen[a] (eV)
$4p^5 5s\ ^1P_1$	1	36.24	36.24	36.24	36.24	35.135
$4p^5 5s\ ^3P_1$	2	35.13	35.13	35.13		
$4p^5 5s\ ^3P_2$	3	35.03				
$4p^5 5s\ ^3P_0$	4	35.94				
$4p^5 4d\ ^3D_1$	5	35.48	35.48	35.48		
$4p^5 4d\ ^1P_1$	6	39.38	39.39	39.39	39.38	39.409
$4p^5 4d\ ^3P_1$	7	33.06	33.06	33.06		32.401

[a]Calculated values; the remainder have been observed experimentally.

Thus metastable contributions to the overall photoabsorption spectrum are an unwanted but inevitable occurrence. From the collisional radiative (CR) model of Colombant and Tonon [36], one can deduce the electron temperature T_e in the plasma using the equation for irradiation at a laser wavelength λ (1.064 μm)

$$T_e = 5.2 \times 10^{-6} Z^{1/5} (\lambda^2 \phi)^{3/5}, \tag{1}$$

where Z is the atomic number, ϕ is the mean laser power density. From this model, $T_e \sim 1.5$ eV in our experiment. Assuming a simple Boltzmann distribution, this equates to ~30% population distribution in the first two excited states given above. Separate calculations were performed to isolate the metastable regions in the spectrum from ground state absorption to assist in the identification of transitions. Figure 3 displays the results. Calculations were performed from the ground state and metastable states ($4p^6 4d$) separately to the upper state levels listed at the start of this section. This was for ease of comparison between the calculated and observed spectrum and a calculation performed to the listed upper states from both the ground and $4p^6 4d$ metastable state was found to have little effect on the energy positions. The series limits proposed were obtained by a least squares fit to the respective quantum defects.

When trying to match experimental peaks to the computed levels, *jj* coupling managed to predict the energy values for the higher members of certain Rydberg series well and gave purities greater than 65% for some of the levels. However, for some of the early series members, *LS* coupling proved more reliable; see Table I. In particular, the energy levels calculated for the $4p^5 4d5s$ configuration are shown with the *jj* and *LS* labels. Through comparisons with the experimentally observed energy levels by Lyon *et al.* [32] and Mansfield and Newsom [2], the *LS* coupling labeling is most accurate for this configuration. It was therefore optimal

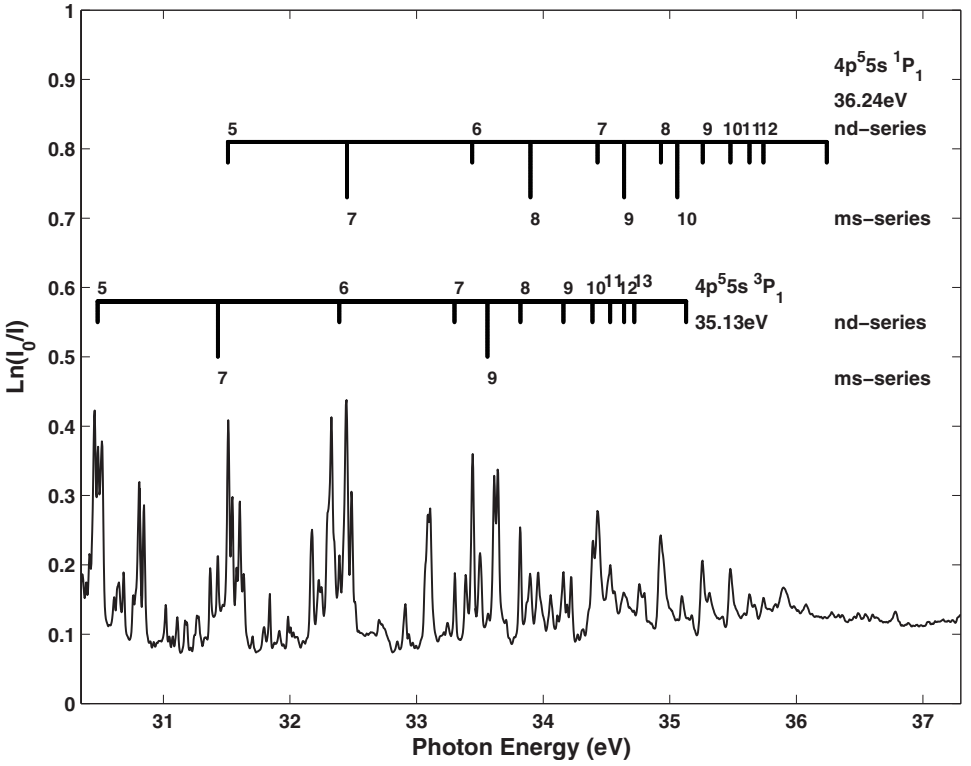

FIG. 4. Photoabsorption spectrum of Sr II from 30.35 to 36.30 eV with the $(4p^5 5s\ ^1P)nd$, $ms\ ^2P$ series converging on the $4p^5 5s\ ^1P_1$ and $4p^5 5s\ ^3P_1$ core at 36.24 and 35.13 eV, respectively.

TABLE III. Observed and calculated energies for the $4p^6 5s \rightarrow 4p^5 5s\ nd, ms$ transitions of Sr II.

Level	E_{exp} (eV)	E_{calc} (eV)	gf	n^*	$jj^{\dagger}/LS^{\S}$ coupling
		$4p^5 5s\ (^1P_1)\ nd\ ^2P_{1/2}$ series to limit (1) 36.24 eV			
5*d*	31.51	31.58	0.2330	3.39	§23.4% $5s5d\ (^1P)$−17.8% $4d9s\ (^3P)$
6*d*	33.44	33.43	0.0669	4.41	§22.3% $5s6d\ (^1P)$−17.0% $5s8d\ (^3P)$
7*d*	34.43	34.62	0.1385	5.48	§14.1% $5s7d\ (^1P)$−12.6% $4d10s\ (^3D)$
8*d*	34.93	34.87	0.1481	6.45	§29.5% $5s8d\ (^1P)$+24.4% $4d6s\ (^1P)$
9*d*	35.26	35.25	0.1192	7.45	§17.0% $5s9d\ (^1P)$−13.0% $4d6s\ (^1P)$
10*d*	35.48	35.42	0.0940	8.46	§29.1% $5s10d\ (^1P)$+21.3% $5s10d\ (^3P)^4D$
11*d*	35.63	35.55	0.0846	9.44	§32.1% $5s11d\ (^1P)$+22.8% $5s11d\ (^3P)^4D$
12*d*	35.74	35.65	0.0669	10.43	§33.3% $5s12d\ (^1P)$+24.1% $5s12d\ (^3P)^4D$
13*d*	35.83	35.73	0.0566	11.52	§24.7% $5s13d\ (^1P)$−10.9% $5s13d\ (^3P)^2D$
14*d*	35.89	35.79	0.0530	12.47	§29.5% $5s14d\ (^1P)$+21.6% $5s14d\ (^3P)^4D$
		$4p^5 5s\ (^1P_1)\ ns\ ^2P_{1/2}$ series to limit (1) 36.24 eV			
5*s*	23.46[a]	23.42	0.1686	2.06	†76.6% (^1P)−4.8% $4d^2\ (^1S)$
6*s*	29.33	30.27	0.0074	2.81	†33.3% $5s6s\ (^1P)$−11.4% $4d5d\ (^3D)^4D$
7*s*	32.45	32.88	0.0014	3.79	†44.8% $5s7s\ (^1P)$+14.9% $4d6d\ (^3P)^2P$
8*s*	33.90	33.97	0.0122	4.82	†78.6% $5s8s\ (^1P)$+3.0% $5s9d\ (^3P)^4D$
9*s*	34.64	34.57	0.0028	5.83	†81.9% $5s9s\ (^1P)$+4.3% $4d10d\ (^3D)^2S$
10*s*	35.06	34.94	0.0019	6.79	†94.1% $5s10s\ (^1P)$
		$4p^5 5s\ (^3P_1)\ nd\ ^4F_{3/2}$ series to limit (2) 35.13 eV			
5*d*	30.48	30.58	0.1724	3.42	†19.1% $5s5d\ (^3P)$+7.2% $4d5d\ (^3F)^4P$
6*d*	32.39	32.52	0.4802	4.45	†29.5% $5s6d\ (^3P)$+10.6% $5s6d\ (^3P)^4D$
7*d*	33.30	33.24	0.0062	5.44	†32.3% $5s7d\ (^3P)$−17.9% $4d7d\ (^3F^4F)$
8*d*	33.82	33.82	0.1420	6.42	†54.3% $5s8d\ (^3P)$−11.6% $5s9d\ (^3P)^4D$
9*d*	34.16	34.10	0.0043	7.45	†44.6% $5s9d\ (^3P)$−15.4% $5s7d\ (^1P)^2P$
10*d*	34.39	34.30	0.0186	8.52	†41.7% $5s10d\ (^3P)$−26.6% $5s7d\ (^3P)^2P$
11*d*	34.53	34.60	0.0935	9.45	†44.8% $5s11d\ (^3P)$−15.4% $5s13d\ (^1P)^2P$
12*d*	34.64	34.65	0.0134	10.44	†37.2% $5s12d\ (^3P)$+28.5% $5s15d\ (^1P)^2P$
13*d*	34.72	34.73	0.0806	11.39	†57.5% $5s13d\ (^3P)$−18.1% $5s14d\ (^3P)^2P$
		$4p^5 5s\ (^3P_1)\ nd\ ^4P_{3/2}$ series to limit (2) 35.13 eV			
4*d*	21.37[a]	21.27	0.0015	1.99	§92.9% $5s4d\ (^3P)$
5*d*	30.42	30.18	0.0084	3.40	†25.3% $5s5d\ (^3P)$−11.4% $4d6s\ (^3D)^4D$
6*d*	obscured	32.32	0.0006		†18.0% $5s6d\ (^3P)$−15.4% $5s6d\ (^1P)^2P$
7*d*	33.25	33.26	0.0100	5.37	†25.0% $5s7d\ (^3P)$−21.2% $5s6d\ (^3P)^4D$
8*d*	obscured	33.77	0.0001		†72.7% $5s8d\ (^3P)$−13.1% $5s8d\ (^1P)^2P$
9*d*	obscured	34.09	0.0046		†49.0% $5s9d\ (^3P)$+20.5% $5s8s\ (^3D)^4D$
		$4p^5 5s\ (^3P_2)\ nd\ ^2P_{1/2}$ series to limit (3) 35.03 eV			
4*d*	21.81[a]	21.70	0.0077	2.03	§87.9% $5s4d\ (^3P)$+3.4% $5s^2\ (^2P)^2P$
5*d*	30.39	30.50	0.1691	3.42	§28.3% $5s5d\ (^3P)^4D$+15.7% $4d6d\ (^3P)^2P$
6*d*	32.25			4.42	
7*d*	33.19	33.13	0.0347	5.44	§51.4% $5s7d\ (^3P)$−10.1% $5s6d\ (^3P)^4D$
8*d*	33.72	33.70	0.1070	6.44	§33.2% $5s8d\ (^3P)$−9.5% $4d7d\ (^3D)^4D$
9*d*	34.06	33.97	0.0625	7.48	§51.9% $5s9d\ (^3P)$−8.6% $5s9d\ (^3P)^4D$
10*d*	34.27	34.15	0.0199	8.45	§59.5% $5s10d\ (^3P)$−11.4% $5s10d\ (^3P)^4D$

TABLE III. (*Continued.*)

Level	E_{exp} (eV)	E_{calc} (eV)	gf	n^*	$jj^{\dagger}/LS^{\S}$ coupling
		$4p^5 5s\ (^3P_2)\ nd\ ^2D_{3/2}$ series to limit (3) 35.03 eV			
5*d*	31.55	31.57	0.1820	3.44	†13.8% $5s5d\ (^3P)^2P$−10.5% $4d7d\ (^3P)^4D$
6*d*	33.39	33.36	0.0458	4.44	†62.1% $5s6d\ (^3P)$+3.2% $5s8d\ (^3P)^2P$
7*d*	34.32	34.30	0.0060	5.44	†39.2% $5s7d\ (^3P)$+30.2% $5s7d\ (^3P)^4P$
8*d*	34.86	34.83	0.0240	6.48	†81.4% $5s8d\ (^3P)$−5.1% $4d10d\ (^3D)^2D$
9*d*	35.18	35.16	0.0040	7.47	†92.0% $5s9d\ (^3P)$
10*d*	obscured	35.37	0.0045		†95.5% $5s10d\ (^3P)$
		$4p^5 5s\ (^3P_2)\ nd\ ^4P_{1/2}$ series to limit (3) 35.03 eV			
4*d*	21.22[b]	21.13	0.003	1.99	§96.4% $5s4d\ (^3P)$
5*d*	30.42	29.87	0.0044	3.43	§27.6% $5s5d\ (^3P)^2P$+22.7% $5s5d\ (^3P)^4P$
6*d*	32.25	32.30	0.0156	4.42	†30.2% $5s6d\ (^3P)$+13.6% $4d9d\ (^3P)^4D$
7*d*	33.22	33.23	0.0032	5.47	†69.4% $5s7d\ (^3P)$+8.3% $4d9d\ (^3D)^4P$
8*d*	33.73	33.76	0.0073	6.45	†81.5% $5s8d\ (^3P)$−2.7% $4d7d\ (^3P)^2P$
9*d*	34.06	34.09	0.0007	7.46	†49.6% $5s9d\ (^3P)$−21.2% $4d8d\ (^3F)^2P$
10*d*	34.28	34.31	0.0001	8.47	†93.7% $5s10d\ (^3P)$
		$4p^5 5s\ (^3P_0)\ nd\ ^4F_{3/2}$ series to limit (4) 35.94 eV			
5*d*	31.34	31.05	0.0138	3.44	§32.8% $5s5d\ (^3P)$+20.6% $5s5d\ (^1P)^2D$
6*d*	33.19	33.17	0.0023	4.45	§34.4% $5s6d\ (^3P)$−15.8% $4d10s\ (^3F)^4F$
7*d*	34.11	34.17	0.0622	5.45	§24.3% $5s7d\ (^3P)$−9.7% $5s10d\ (^3P)^2D$
9*d*	obscured	34.69	0.0380		§19.5% $5s8d\ (^3P)$−7.1% $5s14d\ (^1P)^2P$
10*d*	obscured	35.00	0.0048		§31.1% $5s9d\ (^3P)$+16.2% $4d6s\ (^1P)^2P$
11*d*	35.18	35.28	0.1838	8.45	§34.6% $5s10d\ (^3P)$+8.9% $5s10d\ (^1P)^2D$

[a]Values taken from Lyon *et al.* [32].
[b]Value taken from Mansfield and Newsom [2].

to use the *LS* coupling nomenclature and energy predictions for the first member of the Rydberg series and follow the *jj* coupling results for the higher members. It should be noted that in some cases *LS* coupling provided a better match with experiment and was used throughout the series in those cases. Throughout the paper we have chosen to use *LS* labeling for the series for ease of comparison between this work and the previous work on Sr II described above. It proved useful to compare our photoabsorption spectrum with the absolute photoionization cross section measurements of Lyon *et al.* [32] as their results are not contaminated with metastable structure. Care was taken to select only those peaks in our spectrum that corresponded to those observed in the cross section measurements.

Five series limits can be obtained from previous experimental work on Sr III [37–40]. Persson and Valind [37] studied the emission spectrum of doubly ionized strontium from a sliding spark discharge and observed the $4p^5 5s\ ^1P_1$, $4p^5 5s\ ^3P_1$, $4p^5 4d\ ^3P_1$, $4p^5 4d\ ^3D_1$, and $4p^5 4d\ ^1P_1$ resonance lines. Reader *et al.* [38] studied the resonance-line spectrum from the $4p^6\ ^1S_0$ ground state to the $4p^5 4d$ and $4p^5 5s$ configurations in Rb II through to Mo II using a sliding spark discharge also. The 4*p* photoabsorption spectrum of Sr III was recorded by Kilbane *et al.* [39] which gives a value for the $4p^5 5s\ ^1P_1$ limit and the $4p^5 4d\ ^1P_1$ limit. Hansen [12] computed the $4p^5 4d\ ^1P_1$, $^3P_1$ limits and the $4p^5 5s$ average energy configuration using a least squares fit to the data obtained by Persson. The fitted parameter values were then compared to Hartree-Fock results which were found to be in good agreement. Table II displays the observed series limits in this work and compares them to previous results.

A. The $4p^5 5s\ nd, ms$ series

The 4*p* inner-shell excitation spectrum of Sr II involves four doubly ionized states $4p^5 5s\ ^3P_{2,1,0}$, $^1P_1$ which serve as series limits. In this study, we report on eight $4p^5 5snd, ms$ series converging onto four series limits. Well developed Rydberg series are observed to the singlet based $4p^5 5s\ ^1P_1$ limit, whereas series converging to the $^3P_{2,1,0}$ limits are weak, except for the first few members. The $4p^5 5snd$ series members are stronger than the transitions to the $4p^5 5sms$ levels. A similar observation was made for the 4*p* excitation of Rb I [41]. All the $4p^5 5snd, ms$ levels have well defined and consistent quantum defect numbers. The quantum defects for the *nd* and *ns* series are 1.55 and 3.20, respectively, which compare well with those of Rb I, 1.70 and 3.30 [41].

One of the strongest series observed in the 4*p* photoabsorption spectrum was the $(4p^5 5s\ ^1P)nd\ ^2P$ series. The series was formed using levels calculated under the *LS* coupling

TABLE IV. Observed and calculated energies for the $4p^6 5s \rightarrow 4p^5 4d\ nd, ms$ transitions of Sr II.

Level	E_{exp} (eV)	E_{calc} (eV)	gf	n^*	$jj^{\dagger}/LS^{\S}$ coupling
		$4p^5 4d\ (^3D_1)\ ms\ ^2D_{3/2}$ series to limit (5) 35.48 eV			
6*s*	31.60	30.90	0.0111	3.74	†−43.5% $4d6s\ (^3D)$−6.1% $4d6d\ (^3P)^2D$
7*s*	33.11	32.64	0.0021	4.79	†38.0% $4d7s\ (^3D)$−12.0% $4d7s\ (^3D)^4D$
8*s*	33.82	33.70	0.0131	5.72	†−19.4% $4d8s\ (^3D)$−13.1% $5s9s\ (^3P)^4P$
9*s*	34.30	34.23	0.0015	6.78	†52.6% $4d9s\ (^3D)$−20.4% $5s7d\ (^3P)^2D$
10*s*	34.57	34.62	0.0368	7.72	†23.6% $4d10s\ (^3D)$−15.8% $4d10d\ (^3F)^2P$
		$4p^5 4d\ (^3D_1)\ nd\ ^2D_{3/2}$ series to limit (5) 35.48 eV			
5*d*	31.63	31.27	0.0194	3.76	†−9.4% $4d5d\ (^3D)$+7.8% $5p^2\ (^2D)^2D$
6*d*	33.09	33.03	0.0044	4.77	†15.1% $4d6d\ (^1D)^2P$+9.6% $4d6d\ (^3D)^2D$
7*d*	33.82	33.83	0.0002	5.72	†22.0% $4d7d\ (^3D)$+19.3% $4d7d\ (^1P)^2P$
8*d*	34.27	34.34	0.0015	6.70	†21.0% $4d8d\ (^1P)^2P$+10.7% $4d8d\ (^3D)^2D$
9*d*	34.57	34.66	0.0092	7.72	†28.1% $4d9d\ (^3D)$−25.6% $4d9d\ (^3F)^2D$
10*d*	34.76	34.88	0.0097	8.68	†28.7% $4d10d\ (^3D)$−27.8% $4d10d\ (^3F)^2D$
		$4p^5 4d\ ^1P_1\ ms\ ^2P_{3/2}$ series to limit (6) 39.38 eV			
5*s*	26.972[a]	27.02	1.4561	2.09	§67.1% $5s4d\ (^1P)$+12.0% $5s5d\ (^3P)^2P$
6*s*	35.59			3.79	
7*s*	36.99	37.32	0.0081	4.77	†52.0% $4d7s\ (^3D)^4D$−42.0% $4d7s\ (^1P)^2P$
8*s*	out of range	38.38	0.0017		†52.0% $4d8s\ (^3D)^4D$+42.2% $4d8s\ (^1P)^2P$
		$4p^5 4d\ ^3P_1\ ms\ ^2P_{1/2}$ series to limit (7) 33.06 eV			
6*s*	29.19	27.70	0.0209	3.75	§77.8% $4d6s\ (^3P)$+11.5$ $4d6s\ (^3P)^4P$
7*s*	30.68	29.96	0.0120	4.78	§44.8% $4d7s\ (^3P)$+23.8% $4d7s\ (^3P)^4P$
8*s*	31.43	30.98	0.0092	5.77	§64.7% $4d8s\ (^3P)$+18.6% $4d8s\ (^3P)^4P$
9*s*	31.88	31.52	0.1012	6.79	§27.9% $4d9s\ (^3P)$+12.6% $4d9s\ (^3P)^4P$

[a]Values taken from Lyon *et al.* [32] as doublet could not be resolved in our experiment.

scheme, the main reason being that it provided well-matched values to experimental peaks which in turn produced a regular quantum defect. The previously published limit for the $4p^5 5s\ ^1P$ level at 36.24 eV [18,39] was used in this work as it provided the best fit with experiment as did the $4p^5 5s\ ^3P$ level at 35.13 eV observed by Persson and Valind [37] and Reader [38].

The $(4p^5 5s\ ^1P)ns\ ^2P_{1/2}$ Rydberg series are much weaker than their *nd* counterparts. The *jj* coupling scheme was favored for these levels; the calculated $(4p^5 5s\ ^1P)ns\ ^2P_{1/2}$ levels have high purity for $n > 8$ in *jj* coupling and the energy level predictions matched better. The $4p^5 5s^2$ level had the same calculated energy and mixing in both *LS* and *jj* coupling. The $4p^5 5s^2$ level $^2P_{1/2}$ had 76% purity (configuration interaction from the $4d^2$ level being the most significant). Figure 4 shows the 5*snd*, *ms* Rydberg series converging on the $4p^5 5s\ ^1P_1$ and $^3P_1$ limits.

Fitting a limit to the $(4p^5 5s\ ^3P)nd\ ^4P_{1/2}$ and $^2D_{3/2}$ series gave a new value for the $4p^5 5s\ ^3P_2$ level of Sr^{2+} of 35.03 eV. Our data for the $(4p^5 5s\ ^3P)nd\ ^4P_{3/2}$, $^4F_{3/2}$ series fitted well with the known $4p^5 5s\ ^3P_1$ level at 35.13 eV [37,38]. Peaks from these series were weak with some peaks obscured in the dense bunching of resonances. Although the energy of the $(4p^5 5s\ ^3P)4d\ ^4P$ level was predicted accurately in both *LS* and *jj* coupling (see Table I), the former gave over 90% purity. For the higher $^4P_{3/2}$ members ($n \geqslant 7$), *LS* coupling best labeled the level given in Table III as $(^1P)^2D$. In *jj* coupling, the same calculated energies were labeled as $(^3P)^4P$ states with a higher degree of purity so this coupling scheme was favored for the higher members.

The $(4p^5 5s\ ^3P_2)nd\ ^2D_{3/2}$ series was satisfactorily matched with calculated values in *jj* coupling, again the higher members ($n \geqslant 8$) possessing over 80% purity. The $(4p^5 5s\ ^3P)nd\ ^4F_{3/2}$ Rydberg series members showed a high degree of mixing and *LS* coupling was chosen as it provided the best match with experimental values. This series allowed us to determine the $4p^5 5s\ ^3P_0$ level in Sr III at 35.94 eV.

B. Doubly excited series—$4p^5 4dnd$, *ms*

Three series limits for the doubly excited transitions can be obtained from previous work on Sr III, see Table II. The first member of the $(4p^5 4d\ ^1P)ms\ ^2P_{3/2}$ Rydberg series is the large resonance positioned at ~27 eV; see Fig. 1. Lyon *et al.* [32] could resolve this resonance as the $(4p^5 4d\ ^1P)5s\ ^2P_{3/2,1/2}$ doublet located at 26.95 and 26.972 eV, respectively. The higher members of the $(4p^5 4d\ ^1P)ms\ ^2P_{3/2}$ series are calculated to lie at a higher photon energy range

TABLE V. Observed and calculated energies for the $4p^5 4d^2$ configuration, we propose the *LS* labeling for these peaks; see Sec. III B.

Level	E_{expt} (eV)	E_{calc} (eV)	*gf*	*LS*	*jj*
$4d^2$	26.57	26.67	0.7577	$(^1S)^2P_{1/2}$	$(^3P)^2D_{3/2}$
$4d^2$	27.29	27.31	0.0654	$(^3P)^2P_{3/2}$	$(^3P)^2P_{3/2}$
$4d^2$	27.45	27.43	0.1041	$(^3P)^2P_{1/2}$	$(^1S)^2P_{3/2}$
$4d^2$	27.59	27.58	0.1109	$(^3F)^2D_{3/2}$	$(^1D)^2P_{3/2}$
$5p^{2a}$	29.29	29.20	0.2059	$(^1D)^2D_{1/2}$	$(^3P)^4P_{1/2}$

[a]The strong transition observed at 29.29 eV is tentatively assigned to the $5p^2$ configuration as a strong transition is predicted in both coupling schemes at 29.20 eV.

(>35.5 eV) and so we could only observe up to the $4p^5 4d7s$ member. A large degree of mixing is predicted in *jj* coupling for this series particularly with the $(^3D)^4P$ Rydberg series, as can be seen in Table IV. Two series were observed to converge on the $4p^5 4d\ ^3D_1$ limit at 35.48 eV [37,42]. Both the $(4p^5 4d\ ^3D_1)$ *nd*, *ms* series lie close together. Two peaks in the photoabsorption spectra (33.82 and 34.57 eV) have thus been assigned to members in both these series as we cannot select one series over another. The effective quantum defect numbers (n^*) for these doubly excited series are not as consistent as was the case in the previous section and so the designated labeling is tentative.

The *ns* level converging on the $4p^5 4d\ ^3P_1$ limit at 33.06 eV were determined by comparisons with the results of Lyon *et al.* [32]. As certain peaks present in our photoabsorption spectra were still unassigned and they corresponded to peaks present in the absolute cross section spectrum, this *ns* Rydberg series was chosen in order to produce a quantum defect similar to the other *ns* series. Neither coupling scheme uniquely identified this series and so it is tentatively assigned using the previously observed limit [18,42].

The large peak at 26.57 eV on the lower energy side of the $(4p^5 4d\ ^1P)5s\ ^2P$ doublet belongs to the $4d^2$ configuration and the three strong peaks (27.29, 27.44, and 27.59 eV, respectively) to the higher energy side are also from this configuration. Similar to the case for the $4p^5 4d5s$ configuration, there was little correlation between the labeling in *LS* and *jj* coupling with one or two exceptions. We therefore propose tentative labels (see Table V) for these levels based on the following analysis. Three strong resonances are predicted at 27.31, 27.43, and 27.58 eV, and the $4p^5 4d^2\ (^3P)^2P_{1/2}$ level is predicted in both coupling procedures to lie at 27.31 eV. The next predicted peak at 27.43 eV is labeled as the $4p^5 4d^2$ $(^3P)^2P_{3/2}$ in *LS* coupling and $4p^5 4d^2\ (^1S)^2P_{3/2}$ in *jj* coupling. As the calculated results for the $4p^5 4d5s$ configuration showed, *LS* coupling predicts the doublet components of this configuration accurately, whereas using the *jj* coupling scheme, several doublets are predicted to lie 2–3 eV apart. We thus assume, analogous to that case, that *LS* coupling is most appropriate here. The predicted peak at 27.58 eV is labeled as $(^3F)^2D_{3/2}$ in *LS* coupling. In *jj* coupling this same peak is assigned $(^1D)^2P_{3/2}$, but this was deemed unlikely as it also gave a peak at 23.98 eV this same label. This was further validated in *LS* coupling with the 23.98 eV peak also coming out as $(^1D)^2P_{3/2}$. The peak located at 29.29 eV is tentatively assigned to the $5p^2$ configuration as both coupling schemes predict a strong transition from the ground state to this configuration at 29.20 eV. We do not assign a label to it as there is no clear argument to side with one coupling scheme over the other in this case.

IV. CONCLUSION

In this work, we have recorded the 4*p* photoabsorption spectrum of Sr II and have identified single and double excitations involving the 4*d* and 5*s* subshells. We have identified two levels in Sr III and over 60 transitions have been identified and ordered into 12 Rydberg series converging onto seven different series limits, eight due to 4*p* innershell excitation and four resulting from double excitations. Due to the significant overlap between the 4*d* and 5*s* orbital, strong configuration interaction is present with a high degree of mixing predicted between series making the assignment of levels difficult. With the aid of HF calculations in both *LS* and *jj* coupling we have made tentative assignments to the Rydberg series.

ACKNOWLEDGMENTS

This work was supported by the Irish Government National Development Plan including the Basic Research Grants Scheme of the Irish Research Council for Science Engineering and Technology/Science Foundation Ireland and also the Higher Education Authority Programme for Research in Third Level Institutions.

[1] J. M. Bizau, P. Gérard, F. J. Wuilleumier, and G. Wendin, Phys. Rev. A **36**, 1220 (1987).
[2] M. W. D. Mansfield and G. H. Newsom, Proc. R. Soc. London, Ser. A **377**, 431 (1981).
[3] M. A. Baig, J. P. Connerade, C. Mayhew, and K. Sommer, J. Phys. B **17**, 371 (1984).
[4] G. H. Newsom, Astrophys. J. **166**, 243 (1971).
[5] P. C. Deshmukh and S. T. Manson, Phys. Rev. A **28**, 209 (1983).
[6] M. W. D. Mansfield and G. H. Newsom, Proc. R. Soc. London, Ser. A **357**, 77 (1977).
[7] M. Aymar, J. Phys. B **20**, 6507 (1987).
[8] J. E. Hansen, J. Phys. B **5**, 1083 (1972).
[9] B. Brehm and A. Bucher, Int. J. Mass Spectrom. Ion Phys. **15**, 463 (1974).
[10] H. Hotop and D. Mahr, J. Phys. B **8**, L301 (1975).
[11] G. Wendin, J. Phys. B **6**, 42 (1973).
[12] J. E. Hansen, J. Phys. B **8**, 2759 (1975).
[13] J. P. Connerade and D. H. Tracy, J. Phys. B **10**, L235 (1977).
[14] J. P. Connerade, M. W. D. Mansfield, G. H. Newsom, D. H. Tracy, M. A. Baig, and K. Thimm, Proc. R. Soc. London, Ser. A **290**, 327 (1979).
[15] S. J. Rose, I. P. Grant, and J. P. Connerade, Proc. R. Soc. London, Ser. A **296**, 527 (1980).
[16] W. Mehlhorn, B. Breuckmann, and D. Hausamann, Phys. Scr. **16**, 177 (1977).
[17] J. P. Connerade and M. A. P. Martin, J. Phys. B **12**, L53 (1979).
[18] B. Peart and K. Dolder, J. Phys. B **8**, 56 (1975).
[19] D. L. Moores and H. Nussbaumer, J. Phys. B **3**, 161 (1970).
[20] G. Miecznik, K. A. Berrington, P. G. Burke, and A. Hibbert, J. Phys. B **23**, 3305 (1990).
[21] V. K. Ivanov and J. B. West, J. Phys. B **26**, 2099 (1993).
[22] I. C. Lyon, B. Peart, K. Dolder, and J. B. West, J. Phys. B **20**, 1471 (1987).
[23] A. Hibbert and J. E. Hansen, J. Phys. B **32**, 4133 (1999).
[24] R. A. Roig, J. Opt. Soc. Am. **66**, 1400 (1976).
[25] I. C. Lyon, B. Peart, J. B. West, and K. Dolder, J. Phys. B **19**, 4137 (1986).
[26] M. Kutzner, D. Winn, and S. Mattingly, Phys. Rev. A **48**, 404 (1993).
[27] M. Kutzner, V. Maycock, J. Thorarinson, E. Pannwitz, and J. A. Robertson, Phys. Rev. A **66**, 042715 (2002).
[28] W. Schmitz, B. Breuckmann, and W. Mehlhorn, J. Phys. B **9**, L493 (1976).
[29] M. D. White, D. Rassi, and K. J. Ross, J. Phys. B **12**, 315 (1979).
[30] C. McGuinness, G. O'Sullivan, P. K. Carroll, D. Audley, and M. W. D. Mansfield, Phys. Rev. A **51**, 2053 (1995).
[31] Y. Itoh, T. Koizumi, Y. Awaya, S. D. Kravis, M. Oura, M. Sano, T. Sekioka, and F. Koike, J. Phys. B **28**, 4733 (1995).
[32] I. C. Lyon, B. Peart, and K. Dolder, J. Phys. B **20**, 1925 (1987).
[33] J. T. Costello, J.-P. Mosnier, E. T. Kennedy, G. O'Sullivan, and P. K. Carroll, Phys. Scr. **T34**, 77 (1991).
[34] R. D. Cowan, J. Opt. Soc. Am. **58**, 808 (1968).
[35] R. D. Cowan, *The Theory of Atomic Spectra and Structure* (University of California Press, Berkeley, 1981).
[36] D. F. Colombant and G. F. Tonon, J. Appl. Phys. **44**, 3524 (1973).
[37] W. Persson and S. Valind, Phys. Scr. **5**, 187 (1972).
[38] J. Reader and G. L. Epstein, J. Opt. Soc. Am. **62**, 273 (1972).
[39] D. Kilbane, F. Folkmann, J.-M. Bizau, C. Banahan, S. Scully, H. Kjeldsen, P. van Kampen, M. W. D. Mansfield, J. T. Costello, and J. B. West, Phys. Rev. A **75**, 032711 (2007).
[40] C. E. Moore, *Ionization Potentials and Ionization Limits Derived from the Analyses of Optical Spectra* (National Bureau of Standards, Washington, DC, 1970).
[41] M. A. Baig, M. S. Mahmood, M. Akram, and J. Hormes, J. Phys. B **28**, 1777 (1995).
[42] J. Reader and J. O. Ekberg, J. Opt. Soc. Am. **62**, 464 (1972).